



CHORUS

This is the accepted manuscript made available via CHORUS. The article has been published as:

Raman-like stimulated Brillouin scattering in phononic-crystal-assisted silicon-nitride waveguides

Razi Dehghannasiri, Ali Asghar Eftekhar, and Ali Adibi

Phys. Rev. A **96**, 053836 — Published 15 November 2017

DOI: [10.1103/PhysRevA.96.053836](https://doi.org/10.1103/PhysRevA.96.053836)

Raman-like stimulated Brillouin scattering in phononic-crystal-assisted silicon nitride waveguides

Razi Dehghannasiri, Ali Asghar Eftekhar, and Ali Adibi*

School of Electrical and Computer Engineering, Georgia Institute of Technology, Atlanta, Georgia 30332, United States.

We study theoretically stimulated Brillouin scattering (SBS) in silicon nitride (SiN) waveguides created as a phononic line defect inside a pillar-based phononic crystal membrane of the same material for efficient confinement of the generated acoustic phonons to the optical waveguides. The phononic defect is carefully designed to confine the transversally-resonating breathing acoustic mode inside the phononic bandgap of the host phononic crystal. These breathing acoustic modes are well excited by the fundamental optical modes of the waveguides. By optimizing this structure, we show the possibility of achieving high SBS gain in an integrated platform with full CMOS compatibility with other photonic and electronic functionalities. The combination of low-loss traveling photons and long-lasting resonating phonons in the proposed SiN waveguide paves the way for the demonstration of efficient on-chip SBS devices.

I. INTRODUCTION

Inelastic scattering of light by lattice vibration (so called phonon) falls into two regimes, according to whether the phase shift between the adjacent vibrating lattice sites (i.e., atoms) is negligible or not. In the Brillouin regime, light scattering induces a tiny phase shift between atoms and results in the excitation of acoustic phonons. In the Raman regime, however, the phase shift is non-negligible and light scattering involves optical phonons. Depending on whether the creation of phonons is due to fluctuations or an intense optical force, the scattered light falls in either the spontaneous or stimulated regime, respectively. Similar to optical parametric oscillations (OPOs), the prerequisite to an efficient stimulated Brillouin scattering (SBS) is the precise phase-matching between a pair of optical modes (pump and red-shifted Stokes) and an acoustic mode. In other words,

$$\begin{aligned} \omega_p - \omega_s &= \Omega_m \text{ (energy conservation),} \\ \vec{k}_p - \vec{k}_s &= \vec{K}_m \text{ (momentum conservation),} \end{aligned} \quad (1)$$

in which, $\omega/2\pi$ ($\Omega/2\pi$) and \vec{k} (\vec{K}) are the frequency and wavevector of the optical (acoustic) modes, and p , s , and m denote the pump, Stokes, and acoustic modes, respectively.

Although Brillouin scattering was predicted in the 1920s, the interaction was experimentally confirmed in quartz and sapphire [1] in 1964 following the invention of the laser. Since then, with the advancement in microphotonic and nanophotonic fabrication technologies, devices that meet the essential requirements of SBS process have been progressively enhanced, enabling numerous applications for SBS including narrow-linewidth lasers [2–4], inertial sensors [5], non-reciprocal optical devices [6, 7], GHz-rate comb generation [8–11], and slow light and optical memories

[12–14]. These appealing applications have motivated further investigations of SBS and its implementation in platforms compatible with integrated photonics [15–17] and electronics [18].

Different platforms have been studied for SBS such as chalcogenide glasses [19, 20], Si [15–17], silica [4, 8, 21, 22], and CaF₂ [23] to obtain a large SBS gain, g , and ultimately a very low threshold power, P_{th} , quantified as [15, 24, 25]

$$\begin{aligned} g(\Omega) &= \frac{\omega_o Q_m}{2k_m} |\langle \mathbf{f}, \mathbf{u}_m \rangle|^2 \mathcal{L}_m(\Omega - \Omega_m), \\ P_{th} &= \alpha/g_m, \end{aligned} \quad (2)$$

where $\omega_o/2\pi$ and α are the optical frequency and the optical loss of the waveguide, respectively; \mathbf{f} is the power-normalized optical force vector, and $\Omega_m/2\pi$, \mathbf{u}_m , Q_m , and k_m are, respectively, associated with the resonance frequency, displacement vector, quality factor, and effective stiffness of the acoustic mode m , $g_m = g(\Omega_m)$ and $\mathcal{L}_m(\Omega - \Omega_m)$ is the normalized Lorentzian lineshape with $\mathcal{L}_m(0) = 1$. We assumed $\omega_s = \omega_o$ and $\omega_p - \omega_s \ll \omega_s$ as the SBS frequency spacing between optical pump and Stokes waves is often a few GHz. Once the total SBS gain, $G_{SBS} = g_m P_p$, exceeds the optical loss (α), i.e., there is a net SBS gain, the Stokes wave grows as

$$P_s(L) = P_s(0) \exp(g_m P_p L_{eff} - \alpha L), \quad (3)$$

in which P_p is the (non-depleted) input pump power and $L_{eff} = (1 - \exp(-\alpha L))/\alpha$. Eq. (2) reveals that to achieve the maximum gain (i.e., g_m) the integral overlap between the optical force and the acoustic mode over the cross section of the structure (A) (i.e., $\langle \mathbf{f}, \mathbf{u}_m \rangle = \int_A \mathbf{f}^* \cdot \mathbf{u}_m da$) has to be maximized. This necessitates tight localization of optical and acoustic modes along with a large optical force whose profile matches the displacement profile of the acoustic mode. Additionally, Eq. (2) emphasizes the importance of optical loss and mechanical quality factor in lowering the threshold power. As a result, different materials and designs have been investigated for low-loss tight confinement of optical and acoustic

* Corresponding author: ali.adibi@ece.gatech.edu

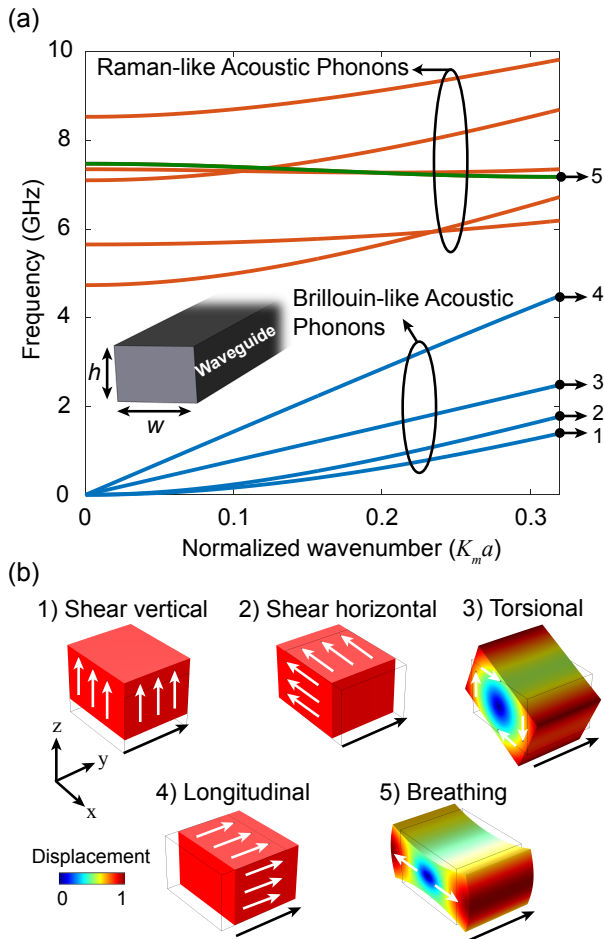


FIG. 1. Phononic dispersion diagram of a free-standing SiN nanowire. (a) Phononic dispersion bands of a nanowire with $(w, h) = (600, 400)$ nm and $(E, \nu, \rho) = (250 \text{ GPa}, 0.25, 3100 \text{ kg/m}^3)$. E , ν , and ρ are Young's modulus, Poisson's ratio, and mass density, respectively. The acoustic wavenumber is normalized to "a", which is the length of the simulated portion of the waveguide (i.e., $a = 500$ nm); Dispersion bands can be classified as Brillouin-like acoustic phonons and Raman-like acoustic phonons based on the starting frequency at $K_m a = 0$. (b) Vibration profiles and propagation direction (i.e., along the y direction) of the acoustic modes of the SiN nanowire at $K_m a = 0.3$ for bands 1–4 and $K_m a = 0.01$ for band 5 in (a). White arrows depict the dominant vibration direction.

waves. To achieve a large optical force, a large refractive index contrast is needed. This is the motivation behind using free-standing Si nanowires [15, 16, 26] that confine both acoustic and optical waves via total internal reflection. However, Si nanowires suffer from linear losses (i.e., scattering loss) and nonlinear losses (such as two-photon absorption (TPA) and TPA-induced free-carrier absorption [15, 27]) that may stifle efficient on-chip SBS generation. Some other proposed platforms like CaF_2 or silica either are not suitable for integrated photonics or possess small refractive index contrasts. Among several alternative materials, silicon nitride

(SiN) is a promising platform as it is fully compatible with integrated photonics technology with a relatively large refractive index, wide transparency window (i.e., from visible to infrared wavelengths), and ultra-low optical losses [28]. Wider transparency window in SiN permits SBS interaction at shorter optical wavelengths (not possible in Si and chalcogenide structures) and allows the use of low-noise solid-state lasers [29, 30] at these wavelengths. In addition, high-tensile stress in low-pressure-chemical-vapor-deposited (LPCVD) SiN allows extremely low phononic losses [31–34], enabling higher SBS gains.

In this paper, we theoretically study SBS for the first time in SiN waveguides and propose a new platform based on the integration of low-loss SiN optical waveguides with phononic crystal (PnC) membranes for confining and engineering the desired acoustic modes. The PnC structure bandgap confines the excited acoustic phonons close to the optical waveguide, leading to the generation of a Stokes wave through SBS with high SBS gains and low threshold powers. In Section II, we first detail the acoustic dispersion diagram of the SiN nanowire and then explain the design of the PnC structure and the line-defect to confine the breathing acoustic mode. In Section III, we discuss the SBS gain in this membrane structure and compare it with a free-standing nanowire with no PnC. Final conclusions are summarized in Section IV.

II. DESIGN OF THE PHONONIC CRYSTAL STRUCTURE

Figure 1(a) shows the schematic of a free-standing SiN nanowire, and the corresponding phononic dispersion diagram of its acoustic modes propagating along the y direction calculated using the finite element method (FEM) in the COMSOL environment [35]. The dispersion diagram is extracted by applying Floquet periodic boundary conditions to the boundaries perpendicular to the y axis (see Fig. 1(b)). Figure 1(b) depicts the displacement profiles of different bands in the nanowire phononic dispersion diagram at normalized wavenumbers $K_m a = 0.01$ and 0.3 . Investigation of the phononic bands starting with $\Omega_m(K_m = 0) = 0$ (i.e., the blue curves in Fig. 1(a)) reveals that the polarization of bands 1 and 2 are shear vertical and shear horizontal, respectively. Band 3 is a torsional mode resulting from mixing bands 1 and 2 via the boundaries of the nanowire, and band 4 is a longitudinal mode. Since the polarizations of bands 1–4 resemble those of the acoustic modes in bulk material (that are utilized in conventional Brillouin scattering), we refer to them as Brillouin-like acoustic phonons. However, the phononic bands with $\Omega_m(K_m = 0) \neq 0$ (i.e., red curves in Fig. 1(a)) resonate transversally between boundaries of the nanowire at smaller wavenumbers and gradually tend to be traveling as wavenumber increases. As these red bands in Fig. 1(a) behave similar to optical phonons in the vicinity of $K_m =$

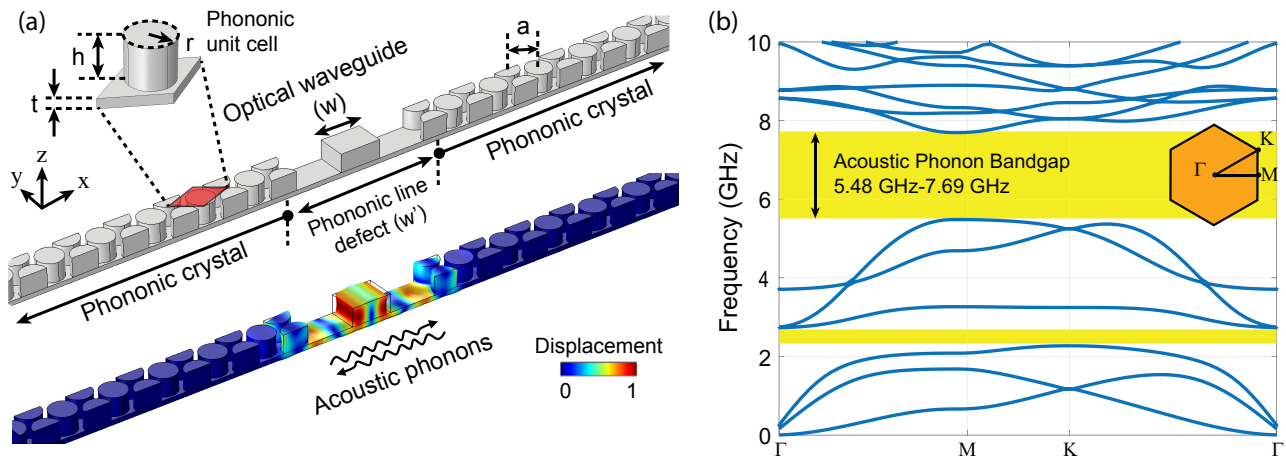


FIG. 2. Proposed SiN structure for the SBS interaction. (a) The schematic of the pillar-based SiN waveguide for SBS generation, showing the phononic crystal and the optical ridge waveguide along with the vibration profile of the breathing acoustic mode confined inside the phononic bandgap of the PnC. The PnC is formed by a triangular lattice of SiN pillars standing on a thin SiN membrane. The phononic line defect is designed such that the breathing vibration is maximized inside the optical waveguide. The displacement profile in (a) is at normalized wavenumber $K_m a \approx 0$. (b) Phononic dispersion diagram of a primitive unit cell of the PnC (highlighted in (a)) over an irreducible Brillouin zone (shown in the inset of (b)). The pillars' height, radius, and membrane thickness are $(h/a, r/a, t/a) = (0.64, 0.44, 0.16)$, respectively.

0, we refer to them as Raman-like acoustic phonons [9]. By expanding the structure from nanowire to bulk with no boundaries, Raman-like acoustic phonons merge with Brillouin-like acoustic phonons and what remain are the three fundamental types of acoustic plane waves: longitudinal, shear vertical, and shear horizontal.

Among Raman-like acoustic modes, the breathing acoustic mode (i.e., the green band 5 in Fig. 1(a)) yields the highest interaction with the fundamental guided photonic mode (i.e., TE_1) of the SiN nanowire. This is because the cross-sectional variation of the displacement profile of these breathing acoustic modes closely matches the profile of the radiation pressure of the photonic mode, which is normal to the surface of the optical waveguide. This greatly enhances the SBS gain (because of $g_m \propto |(\mathbf{f}, \mathbf{u}_m)|^2$) and reduces the threshold optical pump power for nonlinear processes (e.g., phonon lasing) compared to other acoustic modes of the structure. The mechanical resonance frequency of these Raman-like breathing modes in sub-micron-size dimensions for SiN devices falls in multi-GHz frequency ranges.

The need for a mechanical support in a practical structure results in acoustic loss through the support that will reduce the overall SBS gain. To overcome this challenge, in our design, the optimal SiN nanowire is held in place by adding a PnC structure on the two sides (see Fig. 2(a)) exhibiting a phononic bandgap (PnBG) at the desired range of frequencies, which provides the support for the nanowire and yet confines the acoustic phonons to the SiN optical waveguide region at bandgap frequencies for strong photon-phonon interaction. Compared to the structures confining the generated acoustic phonons through the acoustic refractive index contrast between the waveguide and substrate (e.g., [19]), membrane structures enable tighter confinement because there is no

decaying tail for the acoustic modes to the surrounding environment (unless through the membrane). The application of the PnC structure, furthermore, limits the number of confined acoustic modes to those over a certain range of frequencies within the PnBG, culminating in a smaller resonant mode as compared to membrane-based nanowires suspending with arms at far distances [16], which are in general acoustically highly multi-mode. Therefore, PnCs prevent the formation of SBS at frequencies outside the PnBG because of the small overlap between the associated vibration profile with the optical force, which is highly localized to the optical waveguide region, yielding an extremely small SBS gain (i.e., $\langle \mathbf{f}, \mathbf{u}_m \rangle \approx 0$). This minimizes the competition between different acoustic modes in SBS, resulting in SBS with a cleaner spectrum and lower threshold power. The mechanism of phononic confinement in a pillar-based PnC is the Bragg reflection that is enhanced by local resonances of the SiN pillars [36]. Due to the large optical refractive index contrast between SiN and air, a small distance between the PnC structure and the SiN nanowire in Fig. 2(a) is enough to make sure that the guided optical modes of the SiN waveguide do not interact with the PnC pillars. Since the pillars in the structure (see Fig. 2(a)) do not scatter the guided photons, the design of the line defect inside the PnC (which effectively forms a PnC cavity) is independent of the design of the optical (SiN) waveguide. This simplifies the design procedure. To design the PnC cavity, we first optimize a unit cell of the triangular pillar-based PnC (see Fig. 2(a)) to support a wide PnBG with a center frequency close to resonance frequency of the desired breathing acoustic mode of the free-standing SiN nanowire. After designing the unit cell, we create a phononic defect by removing a

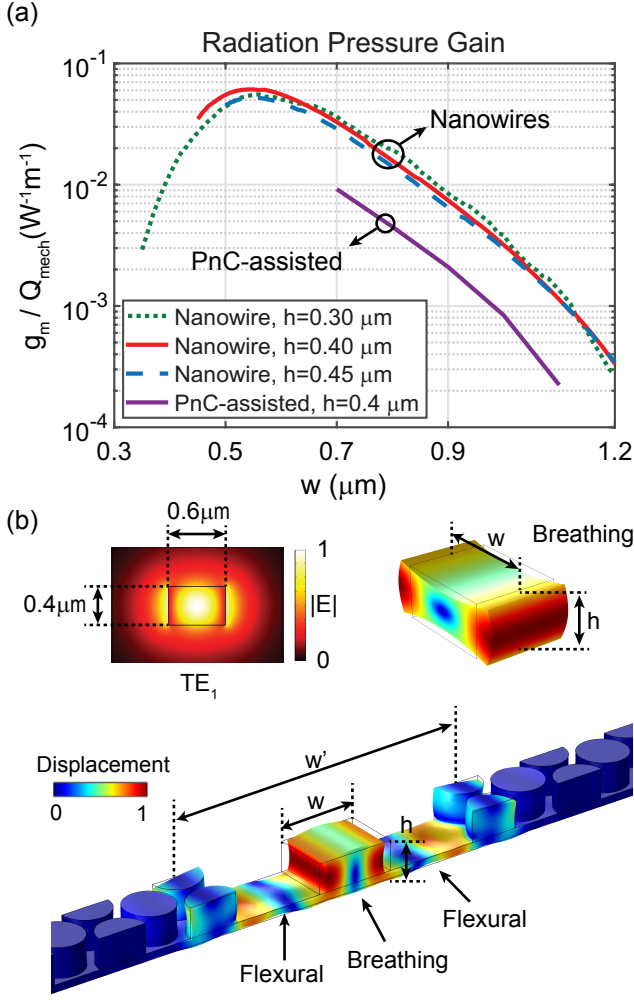


FIG. 3. FSBS gain in SiN nanowires and PnC-assisted SiN waveguides. (a) Variation of the FSBS gain in the SiN nanowire for the acoustic mode shown in (b) as a function of its width (w) for three different heights ($h = 0.3 \mu\text{m}$, $h = 0.4 \mu\text{m}$, and $h = 0.45 \mu\text{m}$). In addition, the FSBS gain for a PnC-assisted waveguide with the total thickness of 400 nm is compared with that of different nanowires. The gain slightly reduces because of the extension of the acoustic waves to the pedestal. (b) The acoustic breathing vibration mode and the electric field of the fundamental TE_1 optical mode (i.e., TE_1 whose electric field lies in the plane of the nanowire) used in the simulation of the FSBS gain of nanowires. In addition, the breathing-like acoustic vibration mode inside the PnC-assisted waveguide is depicted, which is a combination of two primary vibrations: breathing and flexural.

few rows of pillars from the perfect PnC and replacing them with the SiN nanowire (i.e., the center region in Fig. 2(a)). The resulting structure can be visualized as a SiN nanowire with side pedestals surrounded by two perfect PnC regions (see Fig. 2(a)). The width of the PnC line defect is then finely adjusted to support a breathing-like acoustic mode possessing the maximum breathing vibration inside the optical waveguide. For ease of fabrication, we assume the height of the pillars and the waveguide to be identical, which then allows to fabricate the whole structure using a single lithography-and-etching step without the need for separately aligning pillars with the SiN waveguide. This is very important when fabricating a long waveguide as a minor misalignment between the waveguide and the PnC can significantly change the spectrum of SBS and make the Stokes linewidth broader. As an example, using a search through FEM simulations, for the optical waveguide width of $w = 0.7 \mu\text{m}$ (see Fig. 2(a)), we chose $a = 0.5 \mu\text{m}$, $r = 0.22 \mu\text{m}$, $h = 0.32 \mu\text{m}$, and $t = 80 \text{ nm}$ for the PnC structure whose dispersion diagram is shown in Fig. 2(b) demonstrating a large PnBG in the $5.48\text{--}7.69 \text{ GHz}$ frequency range. We also selected the width of the phononic line defect $w' = 2.77 \mu\text{m}$ because it yields stronger breathing vibration inside the selected optical waveguide width, which accordingly maximizes the overlap between the confined acoustic mode and the guided photonic modes in the optical waveguide width of $w = 0.7 \mu\text{m}$.

III. OPTICAL FORCES AND SBS GAIN CALCULATIONS

Traditional SBS theory [37] only captures the bulk-induced nonlinearity (i.e., the electrostriction effect—the material density variation in response to the light intensity, which accordingly affects the material permittivity) and treats optical and acoustic waves as plane waves. However, as the cross-section of the waveguide scales down, plane-wave-approximated SBS is no longer valid because it misses the boundary-induced nonlinearities primarily caused by radiation pressure that plays a major role in SBS at nanoscale structures. Recent studies [24] predict a large enhancement of SBS in nanostructures as a result of the boundary effects, which add to the SBS caused by electrostriction effect. In fact, traveling photons inside a structure with nanoscale cross section exert a noticeable optical pressure normal to the boundaries of guiding region formulated as [25]

$$\mathbf{f}(\mathbf{r}) = \left(\frac{-1}{2} \Delta \epsilon E_{\text{pt}}(\mathbf{r}) E_{\text{st}}^*(\mathbf{r}) + \frac{1}{2} \Delta(\epsilon^{-1}) D_{\text{pn}}(\mathbf{r}) D_{\text{sn}}^*(\mathbf{r}) \right) \hat{\mathbf{n}} \delta(\mathbf{r} - \mathbf{r}_{\Omega}), \quad (4)$$

derived from the Maxwell stress tensors (MSTs). In Eq. (4), E , D , and $\Delta \epsilon$ denote the electric field

amplitude, the electric displacement field amplitude, and the difference in the permittivity across the boundaries,

respectively; subscripts t and n refer to the tangential and normal components, subscripts p and s refer to the pump and Stokes waves, respectively. In addition, \mathbf{r} is the position vector and $\hat{\mathbf{n}}$ represents the unit vector normal to the boundaries of the waveguides; and $\delta(\mathbf{r})$ is the Dirac delta function. The force is non-zero only at the boundaries of the waveguide (i.e., $\mathbf{r} = \mathbf{r}_\Omega$) and pointing from the high-index region (larger ϵ) to the low-index region (smaller ϵ). MSTs can also induce a body force inside optical waveguides if the refractive index varies across the cross-section, which is not the case for our structure.

To calculate the force and the overlapping integral between the optical and acoustic modes of the structure shown in Fig. 2(a), we first use the FEM to simulate the optical and acoustic modes (and their corresponding frequencies and field profiles) using eigen-mode analysis. We then import these modes in the vectorial format into an in-house MATLAB code to calculate the optical force using Eq. (4), and then the overlapping integral between optical and acoustic modes to find the SBS gain as formulated in Eq. (2). Here, we consider forward SBS (FSBS) in which pump and red-shifted Stokes waves are co-propagating. Considering the energy and momentum conservations in FSBS (i.e., Eq. (1)) when pump and Stokes waves are from the same optical dispersion band, we obtain

$$K_m = k_p(\omega_p) - k_s(\omega_s) = \Omega_m \frac{\partial k}{\partial \omega} = \Omega_m / v_g, \quad (5)$$

where v_g is the group velocity of the optical waves. Therefore, to satisfy the phase matching condition in the FSBS, the phononic structure should support an acoustic mode with acoustic phase velocity that matches the group velocity of the engaged optical modes. The nonzero frequency of the Raman-like modes at zero wavenumber and the flat nature of their band structure will ensure the phase matching condition. Owing to the fact that the frequency of the Raman-like breathing acoustic mode is several orders of magnitude smaller than the frequency of the optical pump and Stokes modes (i.e., $(\omega_p - \omega_s)/\omega_p \ll 1$), we can assume in our structure that the optical mode profile of the incident pump and Stokes modes are similar.

Figure 3(a) shows the magnitude of the FSBS gain in free-standing nanowires as a function of the waveguide width (i.e., w) simulated for the breathing acoustic mode at $\lambda_{opt} = 1.55 \mu\text{m}$. As shown in Fig. 3(a), the maximum radiation pressure gain normalized to the mechanical quality factor of the acoustic mode (i.e., g_m/Q_{mech}) is achieved for a SiN waveguide with $h = 400 \text{ nm}$ and $w = 550 \text{ nm}$, which is $g_m/Q_{\text{mech}} = 0.06 (\text{W}\cdot\text{m})^{-1}$. Figure 3(a) highlights the importance of tight localization, i.e., the smaller width of the waveguide results in a larger SBS gain or a stronger photon scattering due to the generated SBS acoustic phonons. For waveguides with widths smaller than $0.5 \mu\text{m}$, the light confinement inside the physical cross section of the SiN nanowire is considerably reduced, resulting in a reduction in the integral overlap of optical and acoustic

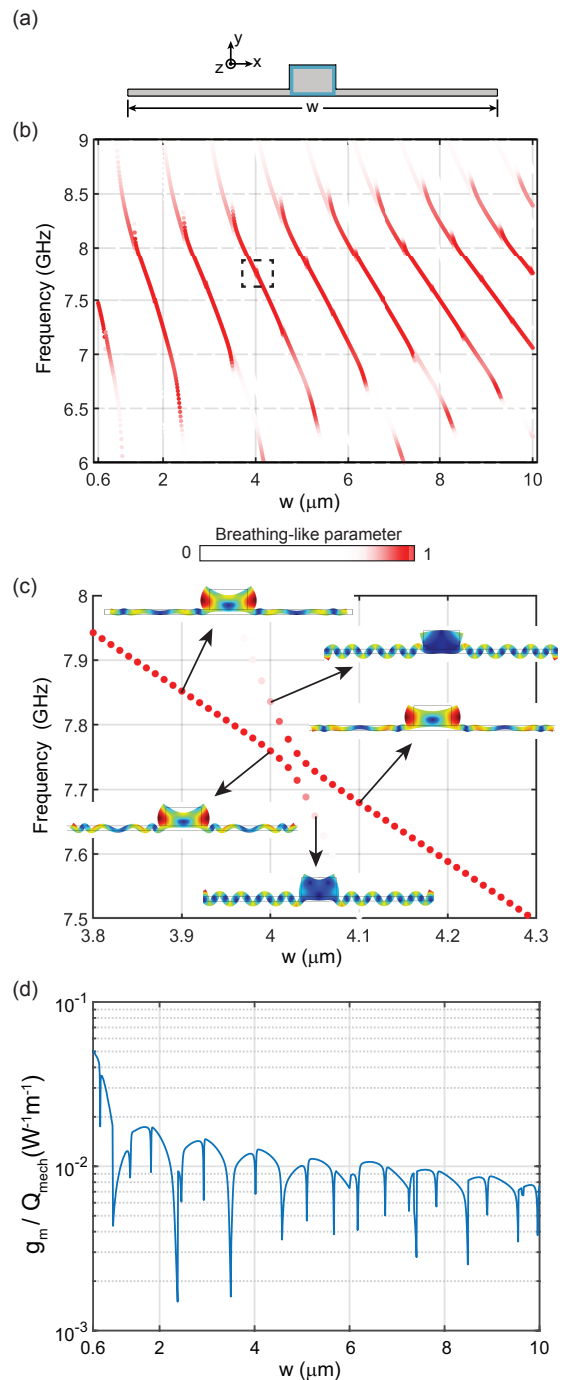


FIG. 4. Properties of a SiN nanowire on a membrane without PnC. (a) The cross-section of the nanowire (height = 400 nm and width = 600 nm) on a membrane with the width of w and the height of 80 nm. (b) The breathing-like acoustic modes of the structure shown in (a) at $K_m = 0$ for different membrane widths. The color code for the representation of the acoustic resonances is the “breathing-like parameter”. (c) Zoomed version of a resonance mode of the structure in (a) in the region identified by the dashed black square in (b) demonstrating mode-splitting (or avoided crossing) due to the coupling between a breathing-like acoustic branch and other acoustic branches of the structure. (d) The FSBS gain calculated for the closest mode of the structure in (a) to the breathing mode of an ideal nanowire (i.e., the mode with the largest “breathing-like parameter” in (b)) as a function of w .

modes, and therefore, the SBS gain. In Fig. 3(a), we also compare the normalized SBS gain (i.e., g_m/Q_{mech}) in the PnC-assisted structure with SiN nanowire. To calculate the gain in the PnC-assisted structure as a function of the width, the PnC is accordingly adjusted to have the breathing frequency at the middle of its PnBG. The smaller value of g_m/Q_{mech} in the PnC-assisted structure can be attributed to the emerging flexural vibration in the pedestal (see Fig. 3(b)), which slightly delocalized the acoustic mode from the optical waveguide. In fact, the flexural vibration does not significantly scatter light compared to breathing vibration because it preserves the total area of the nanowire cross-section. However, the PnC membrane provides loss-less support for the SiN waveguide and better structural stability compared to the bare SiN waveguide with arms at far distances. This enables fabrication of longer SBS waveguides leading to a larger power in the Stokes wave.

It has been shown that the high tensile stress in LPCVD-deposited stoichiometric SiN results in extremely high mechanical quality factors (Q_m -frequency product $> 2 \times 10^{13}$ [33]) at room temperature and (Q_m -frequency product $> 3 \times 10^{15}$ [34]) at millikelvin temperatures in SiN membranes. Therefore, having additional PnC to prevent anchor loss (or phononic leakage) makes $Q_m \approx 10^4$ a reasonable prediction at GHz frequencies for SiN membrane. Therefore, we expect that the SBS gain around $g_m = 600$ can be achieved in tensile-stress SiN. In addition, the presence of the PnC structure eliminates several undesired acoustic modes that naturally exist in the nanowire structures, which can result in the generation of unwanted Stokes modes. Thus, the proposed PnC-assisted structure in this paper improves several properties of a single nanowire for SBS generation.

In order to further highlight the benefits of integrating the membrane structure with PnCs, we also study the FSBS gain in a nanowire sitting on a membrane without PnCs (see Fig. 4(a)). Because the nanowire-on-membrane structure (Fig. 4(a)) with infinite width (w) does not support a breathing mode confined inside the nanowire, we calculate the FSBS gain for membrane structures with finite width. In Fig. 4(b), the acoustic resonances of this structure as a function of w are shown and color-coded based on the “breathing-like parameter”, which is the overlap integral over the region specified in Fig. 4(a) between the normalized field patterns of the acoustic resonance mode of the nanowire-on-membrane structure and that of the corresponding ideal nanowire (a free-standing nanowire with no membrane) with the same height and width. Figure 4(c) illustrates the zoomed version of Fig. 4(b) around $w = 4 \mu\text{m}$, which shows an avoided crossing (or mode splitting) between different acoustic branches. The simulated mode profiles of different points on the band structure in Fig. 4(c) reveals the transition of the acoustic mode families across the

avoided crossing. Figure 4(d) shows variation of the FSBS gain as a function of w for the breathing-like vibration and illustrates that by extending the width of the structure, the FSBS gain reduces owing to the lower concentration of the acoustic mode energy (or power) in the form of breathing vibration inside the optically relevant region (i.e., nanowire). This highlights one of the benefits of the PnC-based structure that enables confinement of the (breathing) acoustic modes to the optical region. In addition, Fig. 4(d) reveals that the FSBS gain drops when breathing acoustic modes transition from one acoustic branch to another acoustic branch of the structure.

We should also highlight that in addition to radiation pressure, electrostrictive force also contributes to the SBS interaction and could be significant as those in silicon nanostructures. However, there is no reported measurement on the photo-elastic coefficients of SiN [38] that allows us to incorporate them in our study.

IV. CONCLUSION

Here, we have proposed a new integrated waveguide platform in SiN for stimulated Brillouin scattering that benefits from low optical losses, wide optical transparency window, and high optical power-handling of SiN, which enables our structure to achieve high total SBS gain (i.e., $G_{\text{SBS}} = g_m P_p$). Additionally, the tensile-stressed LPCVD SiN when accompanied by our designed PnC membrane can lower the SBS threshold power by suppressing phononic leakage. Moreover, the PnC membrane in the proposed SiN waveguides can enhance SBS by: 1) maximizing the overlap between the desired acoustic modes with the optical forces, and 2) reducing the number of unwanted acoustic modes. Minimizing unwanted acoustic modes could also potentially reduce the power budget for the SBS process by eliminating the creation of unwanted Stokes wave from the scattered input pump. Our photonic/phononic platform allows the design of single-mode acoustic waveguides, which benefits applications like GHz-rate comb generation requiring a uniform spacing between combs. Harnessing SBS in SiN enables monolithic integration of SBS devices with on-chip photonics and electronics functionalities, which promises unprecedented on-chip nonlinear optics and GHz signal processing applications in an integrated platform.

V. ACKNOWLEDGEMENT

This work was supported by the Air Force Office of Scientific Research under Grant FA9550-13-1-0032 (Dr. Gernot Pomrenke).

-
- [1] R. Y. Chiao, C. H. Townes, and B. P. Stoicheff, *Phys. Rev. Lett.* **12**, 592 (1964).
- [2] S. P. Smith, F. Zarinetchi, and S. Ezekiel, *Opt. Lett.* **16**, 393 (1991).
- [3] J. Li, H. Lee, and K. J. Vahala, *Opt. Lett.* **39**, 287 (2014).
- [4] W. Loh, A. A. S. Green, F. N. Baynes, D. C. Cole, F. J. Quinlan, H. Lee, K. J. Vahala, S. B. Papp, and S. A. Diddams, *Optica* **2**, 225 (2015).
- [5] F. Zarinetchi, S. P. Smith, and S. Ezekiel, *Opt. Lett.* **16**, 229 (1991).
- [6] J. Kim, M. C. Kuzyk, K. Han, H. Wang, and G. Bahl, *Nat. Phys.* **11**, 275 (2015).
- [7] M. S. Kang, A. Butsch, and P. S. J. Russell, *Nat. Photon.* **5**, 549 (2011).
- [8] P. Dainese, P. S. J. Russell, N. Joly, J. C. Knight, G. S. Wiederhecker, H. L. Fragnito, V. Laude, and A. Khelif, *Nat. Phys.* **2**, 388 (2006).
- [9] M. S. Kang, A. Nazarkin, A. Brenn, and P. S. J. Russell, *Nat. Phys.* **5**, 276 (2009).
- [10] D. Braje, L. Hollberg, and S. Diddams, *Phys. Rev. Lett.* **102**, 193902 (2009).
- [11] R. Pant, E. Li, D.-Y. Choi, C. G. Poulton, S. J. Madden, B. Luther-Davies, and B. J. Eggleton, *Opt. Lett.* **36**, 3687 (2011).
- [12] Y. Okawachi, M. S. Bigelow, J. E. Sharping, Z. Zhu, A. Schweinsberg, D. J. Gauthier, R. W. Boyd, and A. L. Gaeta, *Phys. Rev. Lett.* **94**, 153902 (2005).
- [13] Z. Zhu, D. J. Gauthier, and R. W. Boyd, *Science* **318**, 1748 (2007).
- [14] L. Thevenaz, *Nat. Photon.* **2**, 474 (2008).
- [15] R. Van Laer, B. Kuyken, D. Van Thourhout, and R. Baets, *Nat. Photon.* **9**, 199 (2015).
- [16] H. Shin, W. Qiu, R. Jarecki, J. A. Cox, R. H. Olsson III, A. Starbuck, Z. Wang, and P. T. Rakich, *Nat. Commun.* **4**, 1944 (2013).
- [17] H. Shin, J. A. Cox, R. Jarecki, A. Starbuck, Z. Wang, and P. T. Rakich, *Nat. Commun.* **6**, 6427 (2015).
- [18] J. Li, X. Yi, H. Lee, S. A. Diddams, and K. J. Vahala, *Science* **345**, 309 (2014).
- [19] R. Pant, C. G. Poulton, D.-Y. Choi, H. Mcfarlane, S. Hile, E. Li, L. Thevenaz, B. Luther-Davies, S. J. Madden, and B. J. Eggleton, *Opt. Express* **19**, 8285 (2011).
- [20] T. F. S. Büttner, I. V. Kabakova, D. D. Hudson, R. Pant, C. G. Poulton, A. C. Judge, and B. J. Eggleton, *Sci. Reports* **4**, 5032 (2014).
- [21] M. Tomes and T. Carmon, *Phys. Rev. Lett.* **102**, 113601 (2009).
- [22] H. Lee, T. Chen, J. Li, K. Y. Yang, S. Jeon, O. Painter, and K. J. Vahala, *Nat. Photon.* **6**, 369 (2012).
- [23] I. S. Grudinin, A. B. Matsko, and L. Maleki, *Phys. Rev. Lett.* **102**, 043902 (2009).
- [24] P. T. Rakich, C. Reinke, R. Camacho, P. Davids, and Z. Wang, *Phys. Rev. X* **2**, 011008 (2012).
- [25] W. Qiu, P. T. Rakich, H. Shin, H. Dong, M. Soljačić, and Z. Wang, *Opt. Express* **21**, 31402 (2013).
- [26] E. A. Kittlaus, H. Shin, and P. T. Rakich, *Nat. Photon.* **10**, 463 (2016).
- [27] C. Wolff, P. Gutsche, M. J. Steel, B. J. Eggleton, and C. G. Poulton, *J. Opt. Soc. Am. B* **32**, 1968 (2015).
- [28] Q. Li, A. A. Eftekhar, M. Sodagar, Z. Xia, A. H. Atabaki, and A. Adibi, *Opt. Express* **21**, 18236 (2013).
- [29] A. Schliesser, R. Riviere, G. Anetsberger, O. Arcizet, and T. J. Kippenberg, *Nat. Phys.* **4**, 415 (2008).
- [30] T. J. Kippenberg, A. Schliesser, and M. L. Gorodetsky, *New J. Phys.* **15**, 015019 (2013).
- [31] S. S. Verbridge, J. M. Parpia, R. B. Reichenbach, L. M. Bellan, and H. G. Craighead, *J. Appl. Phys.* **99**, 124304 (2006).
- [32] S. S. Verbridge, H. G. Craighead, and J. M. Parpia, *Appl. Phys. Lett.* **92**, 013112 (2008).
- [33] D. J. Wilson, C. A. Regal, S. B. Papp, and H. J. Kimble, *Phys. Rev. Lett.* **103**, 207204 (2009).
- [34] M. Yuan, M. A. Cohen, and G. A. Steele, *Appl. Phys. Lett.* **107**, 263501 (2015).
- [35] <https://www.comsol.com>.
- [36] R. Pourabolghasem, A. Khelif, S. Mohammadi, A. A. Eftekhar, and A. Adibi, *J. Appl. Phys.* **116**, 013514 (2014).
- [37] R. W. Boyd, *Nonlinear Optics* (Academic, San Diego, 1992).
- [38] K. E. Grutter, M. Davano, and K. Srinivasan, *IEEE J. Sel. Top. Quantum Electron.* **21**, 61 (2015).